Available online at www.sciencedirect.com
ScienceDirect
Bioelectrochemistry 72 (2008) 10–20
Bioelectrochemistry
www.elsevier.com/locate/bioelechem

Spectroelectrochemistry of the redox activation of anti-cancer drug mitoxantrone

Mirela Enache [a], Cezar Bendic [b], Elena Volanschi [b,*]

[a] "I. Murgulescu" Institute of Physical Chemistry, Romanian Academy, Splaiul Independentei 202, Bucharest 060021, Romania
[b] Department of Physical Chemistry, Faculty of Chemistry, University of Bucharest, Blvd. Elisabeta 4-12, Bucharest 030018, Romania

Received 5 July 2006; received in revised form 26 July 2007; accepted 19 October 2007
Available online 6 November 2007

Abstract

The redox behaviour of the anti-cancer drug mitoxantrone was investigated in aprotic media (dimethylsulfoxide-DMSO) by coupled electrochemical and spectral EPR and UV/VIS absorption techniques. The cyclic voltammetry study with stationary and rotating disc electrode (RDE) of the reductive pathway of mitoxantrone points to two-electron transfers and evidences as intermediate species the anion radical, the dianion and the corresponding protonated species. EPR and optical spectra registered during the electrochemical reduction allow the identification of these species and suggest the possibility of back oxidation of the drug by electron transfer to molecular oxygen. The possibility of reductive activation of molecular oxygen by the intermediate species in the redox processes of mitoxantrone is discussed in connection with the cardiotoxicity of the drug. Gas phase and solvent-dependent AM1 and PM3 semiempirical MO calculations allow a rationalization of the experimental results regarding the reactivity in redox processes.

Keywords: Redox activation; Mitoxantrone; Spectroelectrochemistry; PM3 semiempirical calculations

1. Introduction

Mitoxantrone (1,4-dihydroxy-5,8-bis (2-((2-hydroxyethyl) amino)-ethylamino)-9,10-anthracenedione) is an amino-anthraquinone anti-cancer drug synthesized to improve the clinical effectiveness of widely used doxorubicin and other anthracyclines [1]. The drug has major clinical activity in the treatment of several leukaemias and breast cancer [2], the biological activity being assigned to the interaction with DNA and the inhibition of topoisomerase II [3,4].

The metabolism of quinone-containing anti-cancer drugs involves enzymatic reduction of the quinone by one or two electrons, resulting in the formation of the corresponding semiquinone or hydroquinone, respectively. The one electron reduction by a reductase followed by oxidation by molecular oxygen is known as redox cycling and continues until the system becomes anaerobic. In the case of the two-electron reduction, the hydroquinone could become stable and is excreted by the organism in a detoxification pathway [5]. Therefore, the one electron reduction of these drugs is more damaging for biological systems by the possible formation of reactive oxygen species. Early reports indicate that mitoxantrone has a lower risk of cardiac side effects compared with the naturally occurring anthracyclines, doxorubicin and daunorubicin. This is probably due to its smaller tendency to participate to the redox cycling in cardiac mitochondria, being less effective in producing free radicals [6,7]. However, this conclusion has been changed in more recent studies [8,9], which indicate that mitoxantrone causes chronic cardiotoxicity (Fig.1).

The versatility of the electrochemical methods allows to mimic the multitude of biological environments, and in conjunction with spectral and theoretical studies, are a very useful tool for the investigation of the redox behaviour of anti-cancer drugs in anaerobic or aerobic conditions and in different media, and the results may contribute to the understanding of their cardiotoxicity [10].

The aim of the present study is to investigate the redox behaviour of mitoxantrone in dimethylsulfoxide (DMSO), in

* Corresponding author. Fax: +40 21 3159249.
E-mail address: volae@gw-chimie.math.unibuc.ro (E. Volanschi).

1567-5394/$ - see front matter © 2007 Elsevier B.V. All rights reserved.
doi:10.1016/j.bioelechem.2007.10.001

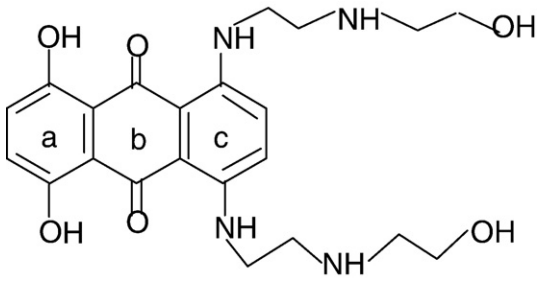

Fig. 1. Chemical formula of mitoxantrone.

order to identify the intermediate species and to examine the possibility of electron transfer from the different intermediates to molecular oxygen. Coupled electrochemical (cyclic and linear voltammetry with stationary and rotating disc electrode, RDE) and spectral (EPR and UV/VIS) techniques were employed. The use of DMSO in our experiments is perfectly justified, as its role as solvent in biological studies, as vehicle for drug therapy and scavenger for reactive oxygen species was recently outlined [11]. Gas phase and solvent-dependent semiempirical MO calculations allow an understanding of the reactivity in redox processes as well as of the possibility of reductive activation of molecular oxygen.

2. Materials and methods

Mitoxantrone was obtained from Sigma. Electrochemical experiments were performed in DMSO spectral grade from Fluka, used without further purification, with 0.1 M tetra-*n*-buthyl ammonium tetrafluoborate ($TBABF_4$) from Fluka as

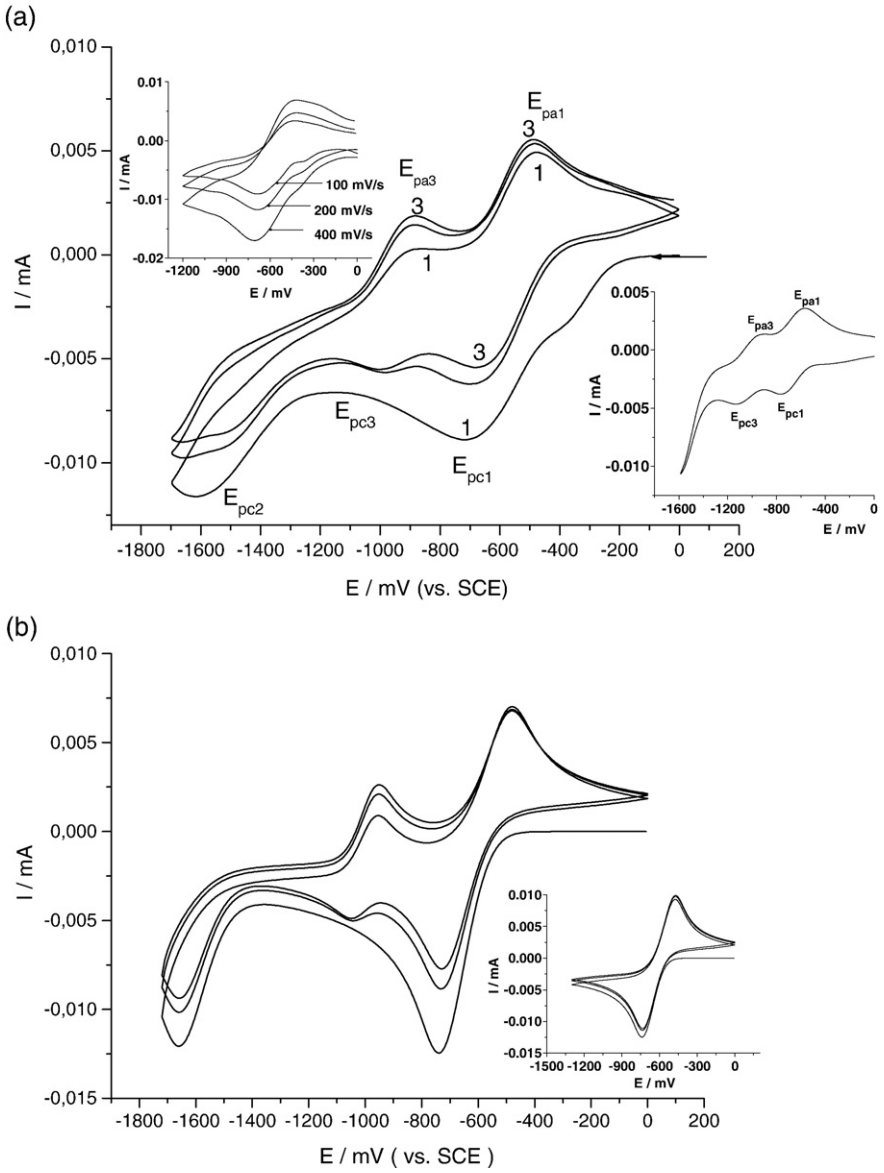

Fig. 2. (a) Cyclic voltammograms of mitoxantrone ($c = 1.34 \times 10^{-3}$ M, $v = 0.2$ V/s) in DMSO, 1–3 successive scans; inset left: cyclic voltammograms in the potential range 0 to −1.2 V at different sweep rates, inset right: first scan of the cyclic voltammogram in the presence of tetrabutylammonium hydroxide (TBOH, $c = 3 \times 10^{-4}$ M). (b) Digisim simulation of the first 3 cycles with the mechanism and parameters in the text, in the potential range 0 to −1.7 V; inset: cycling in the potential range 0 to −1.3 V.

supporting electrolyte, at a VOLTALAB-32 electrochemical device, using a Pt-EDI 101 rotating disc working electrode of 2 mm diameter, a Pt counter electrode and SCE and Ag^+/Ag reference electrodes [12]. The concentration of mitoxantrone solutions used in electrochemical, EPR and spectral experiments was in the range $5\times10^{-5}-5\times10^{-3}$ M.

Experiments were performed at ambient temperature T=293 K (20 °C). Numerical simulations of the voltammograms were performed with the BAS Digisim simulator 3.03, using the default numerical options with assumption of planar diffusion and a Butler–Volmer law for the electron transfer.

The anion radicals for EPR and optical studies were prepared by in situ techniques previously described [13], using the same solvent and supporting electrolyte as for the electrochemical experiments. The EPR spectra were recorded on a JEOL-FA 100 spectrometer in the X-band frequency, using peroxylamine disulphonate as internal standard (a_N=1.3 mT, g=2.0055). The simulation of EPR spectra was performed using the WinSim free software [14]. The optical spectra were registered during the electrochemical and chemical reduction on the Unicam Helios-α and C. Zeiss Jena Specord UV–VIS spectrophotometers.

The semiempirical MO calculations were performed using the AM1 and PM3 hamiltonian in the AMPAC 8 program package and restricted Hartree–Fock (RHF) formalism for closed shell and both restricted (ROHF) and unrestricted (UHF) for open shell structures. Conformational search was performed for the neutral compounds, starting and redox products, in gas phase and in solvent, using the reaction grid option. All structures were fully optimised using eigenvector-following (EF) optimisation algorithm. The influence of the solvent on the electronic structure was considered in the frame of COSMO model [15], implemented into AMPAC, based on the dielectric continuum model. For DMSO a dielectric constant 48.9, refractive index 1.48 and solvation radius 3 Å were used.

3. Results

3.1. Cyclic voltammetry

The cyclic voltammograms of mitoxantrone in DMSO in the electrode potential range $0 \le E/V \le |-1.7|$ are presented in Fig. 2a.

The prewave observed around E=−0.3 V disappears on successive scans and, based on the linear variation of the peak current with the sweep rate, was assigned to an adsorption wave. The redox couple at −0.77 V/−0.42 V (E_{pc1}/E_{pa1}) is characterized by a well shaped anodic counterpart, especially when the potential sweep is reversed after the first reduction peak (Fig. 2a, inset left). The difference between the cathodic and anodic peak potentials at 0.2 V s^{-1}, ΔE_p, allows an estimate of the standard electron transfer rate, k_s, using Nicholson's dimensionless parameter Ψ (Eq. (1)), and the tabulated data providing linking of Ψ to ΔE_p [16,17]:

$$\Psi = \frac{\gamma^{1/2}(\mathrm{RT})^{1/2}k_s}{(nFD_O\pi v)^{1/2}}. \quad (1)$$

In this formula v is the scan rate, $\gamma=D_O/D_R=1$, $D_O=1\times10^{-5}$ cm^2 s^{-1}, n=1 and RT/F=25.67 mV at 298 K (25 °C). A value of $k_s=1.5\times10^{-3}$ cm s^{-1} was obtained, which corresponds to a quasireversible process, assigned to the monoelectronic reduction of the substrate.

The ratio of the peak currents I_{pa}/I_{pc} is smaller than unity, but increases with the sweep rate, and the current function $I_{pc}/v^{1/2}$ decreases slightly with the sweep rate, indicating an EC-type process. The most commonly encountered chemical reaction in electrochemical experiments, even in aprotic media, is the protonation of the anion radical by protic impurities present in the commercially available solvents in amounts of the order of the substrate concentration. The rate constant, evaluated from the dependence of the peak currents ratio on the sweep rate [17], is about 0.13 s^{-1}.

The wave at −1.5 V (E_{pc2}), apparent at the first scan on the voltammogram, has no anodic counter part and the analysis points to a slow electron transfer (ET). From the dependence of the peak potential on the sweep rate, $E_{pc}=f(\log(v/\mathrm{Vs}^{-1}))$, a value of $\alpha\sim0.4$ was obtained. This process was assigned to the reduction of the anion radical of the starting compound to a diamagnetic dianion.

If the potential scan is extended after the potential corresponding to the formation of the dianion, a redox couple around −1.0 V (E_{pc3}/E_{pa3}) appears on subsequent cycles (Fig. 2a). After the second electron transfer, the dianion, which is an electrogenerated base (EGB), shifts the dissociation equilibrium of mitoxantrone (hereafter denoted as AH_2, due to the presence of the dissociable phenol groups) towards the dissociated forms AH^- and H^+. Therefore, this redox couple was assigned to the reduction of the anion AH^-, obtained by the acid dissociation of the substrate, to a dianion radical ($AH^{2-\cdot}$). This assignment is supported by the cyclic voltammograms recorded in the presence of a chemical base, tetrabutylammonium hydroxide (TBOH), when the anion AH^- obtained by the acid dissociation of the phenol groups is already present in solution. In these conditions, this redox couple is evidenced from the first reduction scan (Fig. 2a, inset right).

Based on the upper discussed experimental results, the reductive pathways of mitoxantrone may be synthesized in the following ECECCE reaction sequence:

$$AH_2 + e^- \Leftrightarrow AH_2^{-\cdot} \quad (E) \quad E_1^0 = -0.6\mathrm{V}, \quad k_s = 0.0015\mathrm{cms}^{-1}$$

$$AH_2^{-\cdot} + H^+ \Leftrightarrow AH_3 \quad (C) \quad K_{eq} = 100\mathrm{M}^{-1}\ k_f = 0.13\mathrm{M}^{-1}\mathrm{s}^{-1}$$

$$AH_2^{-\cdot} + e^- \Leftrightarrow AH_2^{2-} \quad (E) \quad E_2^0 = -1.4\mathrm{V}, \quad k_s = 0.0001\mathrm{cms}^{-1}$$

$$AH_2^{2-} + H^+ \Leftrightarrow AH_3^- \quad (C) \quad K_{eq} = 10^4\mathrm{M}^{-1} \quad k_f = 10^5\mathrm{M}^{-1}\mathrm{s}^{-1}$$

$$AH_2 + AH_2^{2-} \Leftrightarrow AH^- + AH_3 (C) \quad K_{eq} = 100\ k_f = 5\mathrm{x}10^5\mathrm{M}^{-1}\mathrm{s}^{-1}$$

$$AH^- + e^- \Leftrightarrow AH^{2-\cdot} \quad (E) \quad E_3^0 = -1.0\mathrm{V}, \quad k_s = 0.01\mathrm{cm/s}$$

The Digisim simulation of the first three cycles starting from the parameters determined by cyclic voltammetry analysis, is

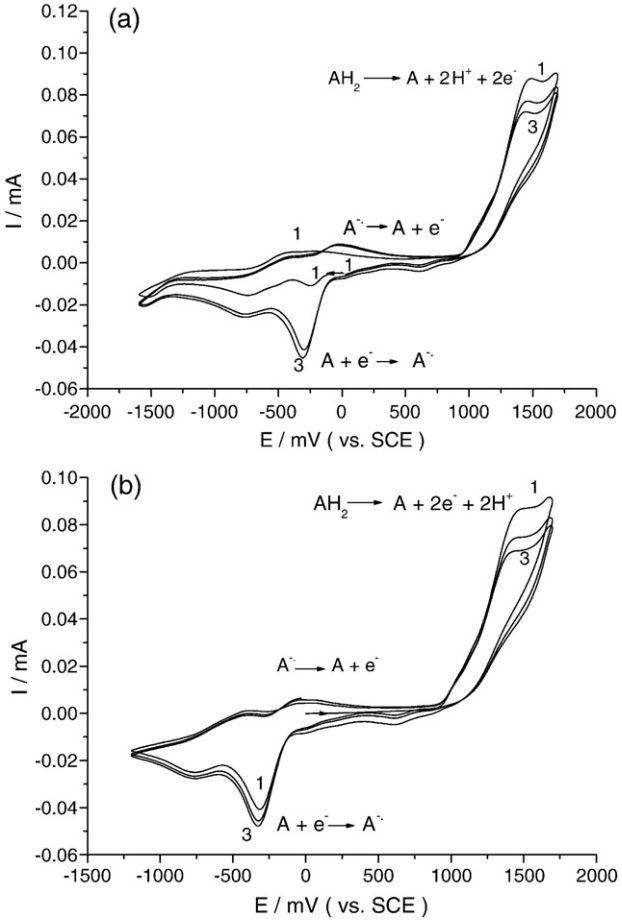

Fig. 3. Cyclic voltammograms of mitoxantrone ($c=1.34\times10^{-3}$ M) in DMSO, with initial reduction sweep (a) and initial oxidation sweep (b), sweep rate $v=0.2$ V/s.

presented in Fig. 2b and supports the proposed reduction mechanism. The standard potentials and electron transfer rates (E^0, k_s) for the electrochemical steps (E), as well as the equilibrium $K_{eq}=k_f/k_b$) and rate constant (k_f) values for the chemical steps (C) deduced from Digisim simulation, are close to the starting values determined by cyclic voltammetry analysis. It should be noted that the standard rate constants obtained for the electron transfers, k_s, are apparent rate constants, not corrected for double layer effects.

Moreover, if cycling is stopped at −1.3 V (inset of Fig. 2b), i.e. before the second ET, the redox couple E_{pc3}/E_{pa3} around −1.0 V, visible on subsequent cycles, is not apparent. This supports the assignment of this couple to the reduction of the anion AH^-, generated by the acid dissociation of the phenol groups of mitoxantrone, under the influence of the EGB dianion (steps 5 and 6 in the scheme above).

If the scan is extended to positive potentials, the aspect of the cyclic voltammogram is different if the potential is initiated with reduction or oxidation.

If the scan is started with reduction (Fig. 3a), on the first scan the adsorption wave and the redox couple corresponding to the monoelectronic reduction of the substrate are observed. At positive potentials an intense oxidation wave is observed, presumably due to the bielectronic oxidation of mitoxantrone to the diquinone or quinone-diimine structure, hereafter denoted by A: $AH_2 \rightarrow A + 2e^- + 2H^+$. On subsequent scans, the new reduction wave at −0.3 V is assigned to the monoelectronic reduction of A. The less negative potential of the couple $A/A^{-\cdot}$ as against that of mitoxantrone (−0.3 V vs. −0.6 V) is in agreement with the stronger electron acceptor character of the diquinone or quinone-diimine structures. Support for this assignment is given by the fact that if the scan is initiated with oxidation (Fig. 3b), the reduction wave of A appears from the first cycle.

3.2. RDE linear voltammetry

The results obtained by RDE linear voltammetry confirm that both reduction steps of mitoxantrone are monoelectronic. From the plot of E vs. $\ln((i_l-i)/i)$ ($N=12$, $R=0.998$), an $E_{1/2}$ value of −0.66 V was obtained for the first electron transfer, in agreement with the value derived from cyclic voltammetry. The plot of the current vs. the square root of the rotating rate (Levich Eq. (2), $N=15$, $R=0.991$) allows the determination of the diffusion coefficient $D_o=5.55\times10^{-5}$ cm^2 s^{-1}. The plot of the reciprocal of the current vs. the reciprocal of the square root of rotating rate (Eq. (3), $N=14$, $R=0.993$) allows the determination of the electron transfer rate and a value of $k_s=1.97\times10^{-3}$ cm s^{-1} was obtained, in good agreement with that obtained by cyclic voltammetry and Digisim simulation. The respective relationships are [17]:

$$i_{lc} = 0.620nFA_0D_O^{2/3}\omega^{1/2}\upsilon^{-1/6}C_O^* \quad (2)$$

$$\frac{1}{i} = \frac{1}{i_k} + \frac{1}{0.620nFA_0D_O^{2/3}\omega^{1/2}\upsilon^{-1/6}C_O^*} \quad (3)$$

where A_0 is the electrode area, ϖ is the rotating rate(s^{-1}), $v=0.01896$ cm^2 s^{-1} the kinematic viscosity of the solvent DMSO) and C_O^* is the bulk substrate concentration (mol/cm^3).

3.3. EPR results

In order to identify the paramagnetic species in the reduction process of mitoxantrone, EPR spectra during the electrochemical and chemical reduction were recorded. In de-aerated DMSO, during the electrochemical reduction at the first wave potential a relatively stable anion radical ($g=2.0053$) is obtained. The experimental spectrum, together with the simulated one and the derived hyperfine constants is presented in Fig. 4.

Assignment of the splitting constants obtained by simulation to the different positions in the molecule is only tentative and was performed by comparison with literature data [7,18,19] and with the calculated spin density pattern. Although the PM3 and AM1 methods are not especially adequate for spin density calculations, we think that the results can give some indication about the delocalization of the odd electron on the different positions of the molecule. Analysis of the ROHF calculated spin density pattern shows that, for the planar moiety

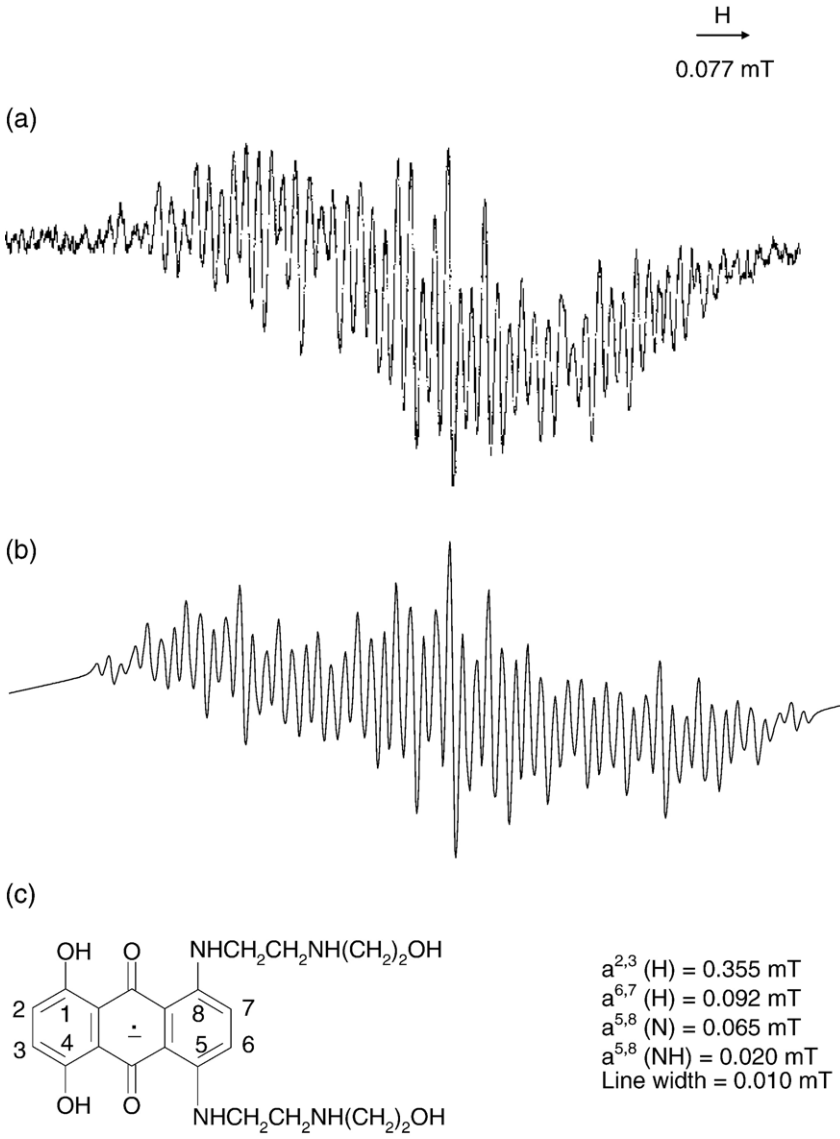

Fig. 4. EPR spectrum recorded at the electrochemical reduction of mitoxantrone ($c=3\times10^{-3}$ M) in DMSO+0.1 M $TBABF_4$, at the potential of the first wave, (a) experimental; (b) simulated; (c) numbering of the different positions of mitoxantrone used in the assignment of the hyperfine splitting constants (see text).

of the molecule, the spin population is almost entirely placed in p_z orbitals, attesting to a π-type radical. The highest spin densities are obtained for the quinone moiety, followed by positions 2,3 and 6,7 in the side rings. Therefore, although all electrons were considered in the present calculations, taking into account the π-character of the anion radical and literature data [20,21], the proton hyperfine splittings, a_H, may be evaluated using the p_z orbital spin density of the carbon atom carrying the proton, ρ_C, and a McConnell type formula:

$$a_H = Q\rho_C \tag{4}$$

where Q is the spin polarization parameter, expressed in magnetic field (induction) units. For the proton, $Q^H{}_{CH}=|2.7|$ mT. For the amine nitrogen a similar relationship may be used with a spin polarization parameter $Q^N{}_{NH}=3.0$ mT and the spin density in the p_z orbital of nitrogen [21].

Evaluation of the hyperfine splittings (hfs) from the theoretical spin densities may be also performed using the UHF calculated spin densities and the relationship:

$$a_X = a^0_X \rho_{Xs} \tag{5}$$

where a^0_X is the calculated value for an isolated atom for which the odd electron resides entirely in the s orbital. The following values were used for hydrogen $a^0_H=50.8$ mT and for the nitrogen atom $a^0_N=54.9$ mT [20].

Both methods reproduce the general trend experimentally observed, but the agreement with the experimental splittings is poor, the calculated hfs being either smaller (0.164/0.165 vs. 0.355 (2H) and 0.099/0.103 vs. 0.092 mT (2H), 0.009/0.013 vs. 0.065 mT (2N), using ROHF spin densities and Eq. (4), or higher than the experimental ones (in the range 1.168 to 1.575 mT, using the UHF spin densities and Eq. (5). The higher

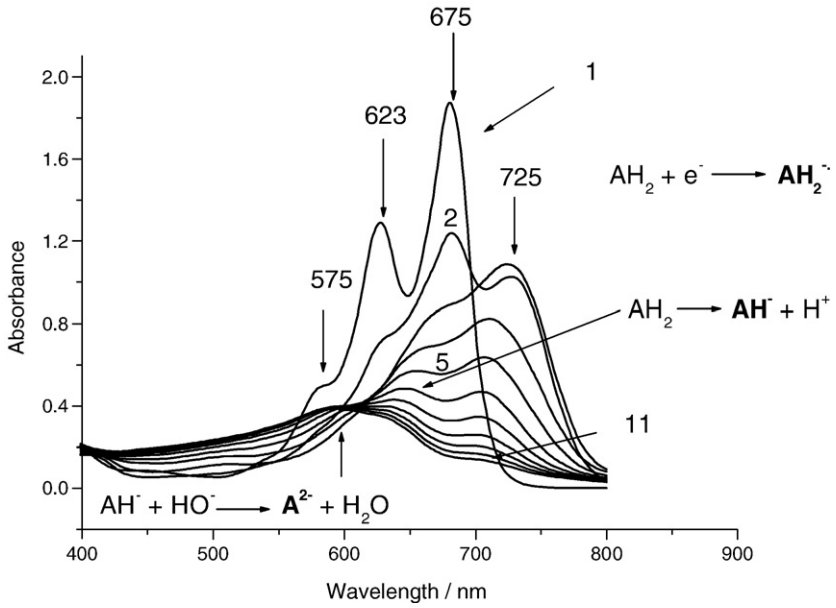

Fig. 5. Absorption spectra recorded for the chemical reduction of mitoxantrone ($c = 1.6 \times 10^{-4}$ M) in DMSO in the presence of different concentrations of TBOH, $c_{TBOH} = 0$ (spectrum 1), $c_{TBOH} = 1.45 \times 10^{-3}$ M (spectrum 11).

hfs constants obtained using UHF spin densities were expected because it is known that UHF calculations without annihilation lead to too large hfs due to spin contamination, in our case $\langle S^2 \rangle$ being in the range 1 to1.34. Both ROHF and UHF calculations predict higher spin densities for sites 2,3 (ring **a**) as against 6,7 (ring **c**) and this difference is enhanced in the solvent-dependent calculations.[1] Therefore, we think as more probable the assignment of the highest splitting (0.355 mT) to the protons in sites 2,3 (ring **a**) and not 6,7 (ring **c**), as previously done [7].

Comparison with literature data on 5,8-dihydroxy-1,4-naphtoquinone and quinizarin (1,4-dihydroxi-9,10-anthraquinone) anion radicals [18,19] shows an increase of the hfs constants of the protons adjacent to the OH groups in the OH-substituted ring from 0.046 to 0.240, for dihydroxy-1,4-naphtoquinone, all four protons becoming equivalent, and from 0.100 to 0.190 mT for quinizarin. Therefore, the preferential delocalization of the odd electron on the OH-substituted ring **a** in the case of the anion radical of mitoxantrone does not seem unreasonable. As the smallest protons hfs are concerned, their assignment to the NH or OH protons is equally probable. Calculated hfs from PM3/DMSO-ROHF spin densities in p_z orbital of the nitrogen atom with a spin polarization parameter $Q_H^{NH} = 3.5$ mT are in reasonable agreement with the experimental ones, i.e. 0.011–0.016 vs. 0.020 mT, whereas no such evaluation is possible for the phenolic protons.

On prolonged electrolysis the spectrum becomes asymmetric, suggesting a mixture of radical species. The lack of symmetry is probably due to the superposition of the dianion radical ($AH^{2-\cdot}$), formed by the reduction of the anion AH^- and evidenced by the cyclic voltammetry on subsequent cycles. Similar EPR spectra but of poorer resolution are obtained in DMSO in the presence of TBOH, even in the absence of electrochemical reduction. Reduction of carbonyl compounds in alkaline media is known to yield anion radicals, but the mechanism is not completely understood [22].

3.4. Absorption spectra

In order to get more information about the redox behaviour of mitoxantrone, optical spectra were recorded during the chemical and electrochemical reduction and oxidation using in situ techniques. In DMSO, in the absence of TBOH, mitoxantrone has absorption bands in the visible region at 675 nm and 623 nm with a shoulder at 575 nm (Fig. 5, spectrum 1).

In the presence of small amounts of TBOH in DMSO (Fig. 5), the absorption bands of the starting compound decrease, and a new absorption maximum at 725 nm appears. This band was assigned to the anion radical of the substrate, based on the similar behaviour observed at the electrochemical reduction and was confirmed by EPR spectroscopy in the same conditions. For TBOH/mitoxantrone molar ratios up to 1:2 (Fig. 5, spectra 2–5) a reversible behaviour is observed, the substrate being entirely recovered by acidifying the solution with water.

For higher TBOH/mitoxantrone ratios (Fig. 5, spectra 6–11), a new band around 650 nm is apparent, and the band of the anion radical of the drug decreases in an irreversible way. This band, visible when the absorption of the drug decreases, was assigned to the AH^- species, formed as result of the dissociation equilibrium of the substrate, which is shifted in the presence of TBOH towards the dissociated forms, AH^- and H^+.

The spectra recorded at the electrochemical reduction of mitoxantrone in DMSO (data not shown) at the potential of the

[1] According to B3LYP/EPR-III//B3LYP/6-311+G** in vacuo calculations of unknown referee, using simplified model compounds (i.e. replacing the NHR functional group by $NHCH_3$), $a_H^{6,7} = -0.255$ mT, $a_H^{2,3} = -0.172$ mT and $a_H^{NH} = -0.062$ mT.

first wave on the voltammogram indicate a similar behaviour as for the chemical reduction in the presence of TBOH. If the current is stopped and the solution is opened to air, this band decreases and the starting compound is recovered, attesting for the reversibility of the first reduction step. A similar absorption range was observed at prolonged electrolysis, in parallel with the dianion formation, which plays the role of electrogenerated base. In strong alkaline media a possible reaction is $AH^- + HO^- \rightarrow A^{2-} + H_2O$, so that the band at about 600 nm was assigned to the A^{2-} species.

If, after the electrochemical reduction and the formation of AH^- and A^{2-} species, the electrochemical oxidation is initiated, the absorption bands of the starting compound are only partially recovered, and a new band appears at 440 nm. This band, which increases on expense of the band at 600 nm, was assigned to species A, resulting from the oxidation of the dianion A^{2-}.

4. Discussion

The experimental data may be rationalized in the following scheme, implying alternative electron and proton transfers. In this scheme AH_2 stands for mitoxantrone, A for diquinone or quinone diimine. The intermediate species were evidenced either by cyclic voltammetry or spectral experiments.

Starting with mitoxantrone, successive electron transfers lead to the anion radical ($AH_2^{-\cdot}$) and dianion (AH_2^{2-}) evidenced by cyclic voltammetry and/or EPR and UV–VIS spectra. These intermediate species act as electrogenerated bases (EGB) and shift the dissociation equilibrium of the phenolic groups towards the phenolate anions (AH^-), which can undergo further monoelectronic reduction to the dianion radical ($AH^{2-\cdot}$), evidenced by EPR spectra in alkaline media.

The oxidative pathways of mitoxantrone: $AH_2 \rightarrow A + 2e^- + 2H^+$ lead to the electroactive species A (diquinone or quinone diimine), which is easily reduced at a potential less negative than the substrate itself to the anion radical ($A^{-\cdot}$) or dianion (A^{2-}). The oxidative pathways are also supported by experimental data (Fig. 3a, b).

4.1. MO calculations

The MO calculations were performed in order to furnish theoretical support for the experimental data previously discussed and to account for the reactivity of the different intermediate species involved in redox processes (Scheme 1), in terms of their electronic structure. At the same time, this is also an attempt to understand at molecular level the possibility of ET from the redox activated species of mitoxantrone to molecular oxygen, presumably responsible for the redox cycling and cardiotoxicity of the drug.

The first problem to be discussed is the choice of the system and the method of calculation. Although calculations on smaller model compounds would in principle be possible in order to save computing time, we have considered in calculations the whole drug molecule, for the following reasons. Preliminary calculations on model compounds for doxorubicin, actinomycin D and mitoxantrone [23,24] have shown that redox properties

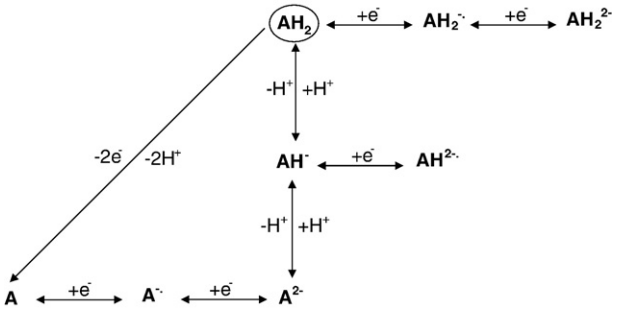

Scheme 1. Possible redox pathways of mitoxantrone in DMSO.

are practically determined by the aromatic moiety. However, it was shown that N-substitution for the amino-anthraquinone drugs may lead to a decrease of the electron affinity and electronegativity, that can result in reduced competition with oxygen for an electron in the mitochondrial electron transport chain, and therefore can influence the cardiotoxicity of the drug [25,26]. On another side, our previous studies on several anti-cancer drugs–DNA interaction (based on a quantum-chemical approach: Mulliken overlap population) have pointed out the importance of the ring substituents in the stabilization of the drug–DNA complexes, by an enhanced contribution of specific hydrogen bonding and other atom–atom intermolecular interactions [27,28]. For these reasons we have considered that quantum solvent-dependent calculations on the whole molecule, including conformational analysis, could bring useful information in the study of the cardiotoxicity of the anti-cancer drugs.

As the method of calculation is concerned, AM1 semiempirical calculations were already used in an attempt to rationalize the redox behaviour of reductively activated quinone derivatives [25,26] and in connection with spectroelectrochemical data on other anti-cancer drugs [29]. From a comparison of AM1 results with ab-initio calculations [26], it was stated that the AM1 method is capable of predicting trends in redox capacity and reactivity of substituted quinone drugs. Recently, it was shown that the PM3 method gives better results than AM1, especially in solvent-dependent calculations on complex organic molecules. In the present work, both AM1 and PM3 calculations were performed. Comparison of the results shows only minor differences in the calculation of redox properties, but more important in the evaluation of the ET towards molecular oxygen. Therefore, in the followings only PM3 results will be discussed.

The following strategy was adopted in our calculations:

– in a first step, a conformational search in both gas phase and solvent (DMSO) was performed for the neutral compounds, starting drug and its oxidation products, using the reaction grid option, in order to obtain the most stable few conformers.
– starting from these conformers, gas phase and solvent-dependent optimisation was performed for the neutral compounds (mitoxantrone, diquinone, quinone diimine), as well as for the intermediate species and products involved in

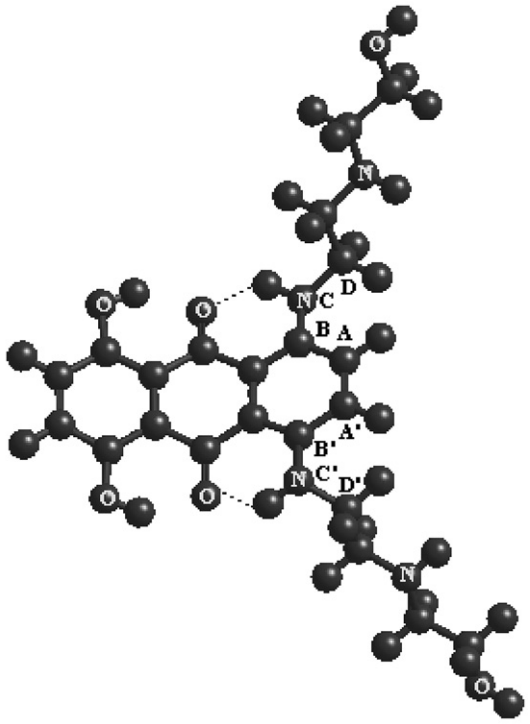

Fig. 6. The structure of the mitoxantrone conformer in DMSO, corresponding to the lowest energy in Table 1, in respect with the rotation around –N–C_{ar} bonds; the position of the side chains is determined by the dihedral angles ABCD, A'B'C'D'.

redox processes, evidenced by experimental data (Scheme 1). Restricted Hartree–Fock (RHF) formalism for closed shell and both restricted (ROHF) and unrestricted (UHF) for open shell structures were employed.

– in a last step, the different calculated electronic properties (charges, spin densities, energies and shape of frontier molecular orbitals, redox properties) were discussed in connection with experimental data, and the possibility of ET to molecular oxygen was analysed.

4.1.1. Geometry optimisation of the neutral compounds

PM3 conformational search of the molecular structure of mitoxantrone and its oxidation products (diquinone, quinone diimine) was performed in gas phase and DMSO in respect with the rotation of the side chains around –N–C_{ar} bonds (dihedral angles ABCD, A'B'C'D', Fig. 6) for mitoxantrone and diquinone, and around =N–CH_2– bonds, in the case of quinone diimine.

The differences between the energies of the different conformers are only 4–12 kJ mol^{-1}, due to the quasi-free rotation of the side chains for a rotation angle in the range −120÷120. The calculated heats of formation, ΔH^f, of the mitoxantrone conformers corresponding to the minima on the grid in gas phase and DMSO are presented in Table 1, together with the characteristic geometrical parameters (the dihedral angle values and the distance between the amine proton and the carbonyl oxygen). It may be observed that the most stable conformer in Table 1, in both gas phase and DMSO, is characterised by the N–H bond directed towards the carbonyl oxygen and a CO... HN distance of about 1.85 Å, ensuring strong hydrogen bonding. Therefore, the position of the saturated side chains in the lowest energy conformers is determined by the hydrogen bonds between the amino and carbonyl groups.

4.1.2. Redox properties of neutral compounds

Relevant electronic parameters used in the discussion of reactivity in redox processes are [25,26]:

– the absolute (vertical) electronegativity (X_v), defined as: $X_v = 1/2(IP + EA)$ or, taking into account Koopman's theorem: $X_v = -1/2(\varepsilon_{HOMO} + \varepsilon_{LUMO})$, where ε_{HOMO} and ε_{LUMO} are the energies of the highest occupied and lowest empty molecular orbitals.

– the adiabatic ionisation potential (IP_{ad}), calculated as the variation of enthalpy (ΔH) in the reaction: $X \rightarrow X^{+\cdot} + e^-$

– the adiabatic electron affinity (EA_{ad}), defined as the negative of enthalpy variation ($-\Delta H$) in the reaction: $X + e^- \rightarrow X^{-\cdot}$

– the adiabatic electronegativity (C_{ad}), calculated as: $X_{ad} = 1/2(IP_{ad} + EA_{ad})$

The heats of formation, the relevant orbital energies and the vertical and adiabatic electronegativities and ionisation

Table 1
Calculated enthalpies of formation, ΔH^f, dihedral angles ABCD and A'B'C'D' (defined in Fig. 6), and the distance between the amine proton and the carbonyl oxygen, for the four lower energy conformers of mitoxantrone, in respect with the rotation around the –HN–C_{ar} bonds

	Gas phase			DMSO		
	ΔH^f (kJ/mol)	ABCD; A'B'C'D'	$d_{H...O=C}$ (Å)	ΔH^f (kJ/mol)	ABCD; A'B'C'D	$d_{H...O=C}$ (Å)
1	−859.95	35; −36	1.83; 1.83	−923.09	−30; −30	1.85; 1.83
2	−855.72	−36; 36	1.83; 1.83	−918.48	40; −40	1.84; 1.83
3	−853.33	−37; −36	1.82; 1.83	−915.26	−30; 40	1.85; 1.84
4	−853.12	36; 37	1.83; 1.82	−910.31	50; 50	1.83; 1.84

Table 2
Gas phase and DMSO-PM3 calculated enthalpies of formation, ΔH^f, energies of the frontier molecular orbitals, ε_{HOMO} and ε_{LUMO}, adiabatic ionisation potentials, IP_{ad}, and electron affinities, EA_{ad}, vertical X_v, and adiabatic X_{ad} electronegativities, and experimental reduction potentials for mitoxantrone, diquinone and quinone diimine

Compound	ΔH^f (kJ/mol)	ε_{HOMO} (eV)	ε_{LUMO} (eV)	X_v (eV)	IP_{ad} (eV)	EA_{ad} (kJ/mol)	X_{ad} (eV)	E_1^0 (V)
Mitoxantrone								
Gas phase	−859.95	−8.35	−1.73	5.04	7.27	228.35	4.82	−0.60
DMSO	−923.09	−8.49	−1.81	5.15	5.93	382.75	4.95	
Diquinone								
Gas phase	−655.27	−8.53	−2.09	5.31	7.41	289.48	5.20	−0.30
DMSO	−746.86	−8.79	−2.39	5.59	6.19	464.21	5.50	
Quinone diimine								
Gas phase	−636.29	−8.94	−1.88	5.41	8.28	247.12	5.42	−0.30
DMSO	−716.65	−9.28	−2.05	5.67	6.70	413.59	5.49	

Table 3
PM3 calculated reaction enthalpies, Δ^rH, for the different reduction and oxidation steps (Scheme 1) for mitoxantrone (AH_2), diquinone and quinone diimine (A), in gas phase and DMSO

Step	Δ^rH (kJ/mol)[a] (gas phase)	Δ^rH (kJ/mol)[a] (DMSO)
$AH_2+e^-\rightarrow AH_2^{-\cdot}$	−228.35	−382.75
$AH_2+2e^-\rightarrow AH_2^{2-}$	−135.71	−711.54
$AH_2\rightarrow AH^-+H^+$	−100.72	−310.98
$AH_2\rightarrow A+2H^++2e^-$		
A=diquinone	204.68	176.23
A=quinone diimine	223.66	206.44
$A+e^-\rightarrow A^{-\cdot}$	−289.48	−464.21
(diquinone)		
(quinone diimine)	−247.12	−413.59
$A+2\ e^-\rightarrow A^{2-}$	−234.97	−834.14
(diquinone)		
(quinone diimine)	−157.87	−761.74

[a] $\Delta^rH=\Sigma\Delta H^f_{Prod}-\Sigma\Delta H^f_{React}$.

potentials for mitoxantrone, diquinone and quinone diimine (the possible oxidation products of mitoxantrone), in both gas phase and in a polar solvent (DMSO) are presented in Table 2.

The results indicate enhanced redox properties of mitoxantrone, diquinone and quinone diimine in DMSO, as against the gas phase, reflected in lower ionisation potential, higher electron affinity and higher vertical and adiabatic electronegativities. The values of ε_{LUMO}, EA_{ad}, X_v and X_{ad} attest that diquinone or quinone diimine are more reducible than mitoxantrone, in agreement with the cyclic voltammetry results, which indicate a less negative reduction potential for diquinone or quinone diimine. Moreover, the adiabatic and absolute electronegativities are close to one another, indicating that no significant geometry modifications arise in the anion radical as against the starting molecule.

The redox pathways (Scheme 1) as evidenced by experimental data may be considered as a sequence of electron and proton transfers. Therefore, the energetics of the different steps was analysed using the values of the formation enthalpies calculated for all intermediate species, in gas phase and DMSO, and the results are contained in Table 3.

Examination of the results in Table 3 shows that the mono and bielectronic reduction steps of mitoxantrone are energetically favourable in gas phase and especially in DMSO. The acid dissociation of the substrate is also exothermic. The reduction of diquinone or quinone diimine (A) to the corresponding anion radical and dianion is more exothermic compared with mitoxantrone, in agreement with the less negative reduction potential evidenced by cyclic voltammetry ($E=-0.30$ V vs. $E=-0.60$ V). The oxidation of mitoxantrone to diquinone or quinone diimine is endothermic, in agreement with its high positive oxidation potential, $E=+1.45$ V.

As far as the influence of the solvent is concerned, the dielectric continuum model is too simple to account for the specific effect of the solvent. However, it may be noted that, as expected, the charged species are stabilized more than neutral ones, and that the reaction enthalpies are more negative in DMSO as compared to the gas phase.

The bielectronic oxidation of mitoxantrone may involve either the hydroxyl groups on ring **a** leading to a diquinone, or the amino groups on ring **c**, resulting in a quinone-diimine structure.

Analysis of the frontier molecular orbitals of mitoxantrone (Fig. 7) indicates that the HOMO orbital is mainly delocalised on ring **c** and amino groups, whereas the LUMO is mainly delocalised on ring **b**. Therefore, we may infer that the quinone moiety should be responsible for the behaviour in reduction processes, whereas the amino substituents on ring **c** are expected to be involved in oxidation processes.

Comparison of the calculated reaction enthalpies for the two oxidation products (Table 3) shows that oxidation pathways in gas phase and DMSO are slightly more endothermic for

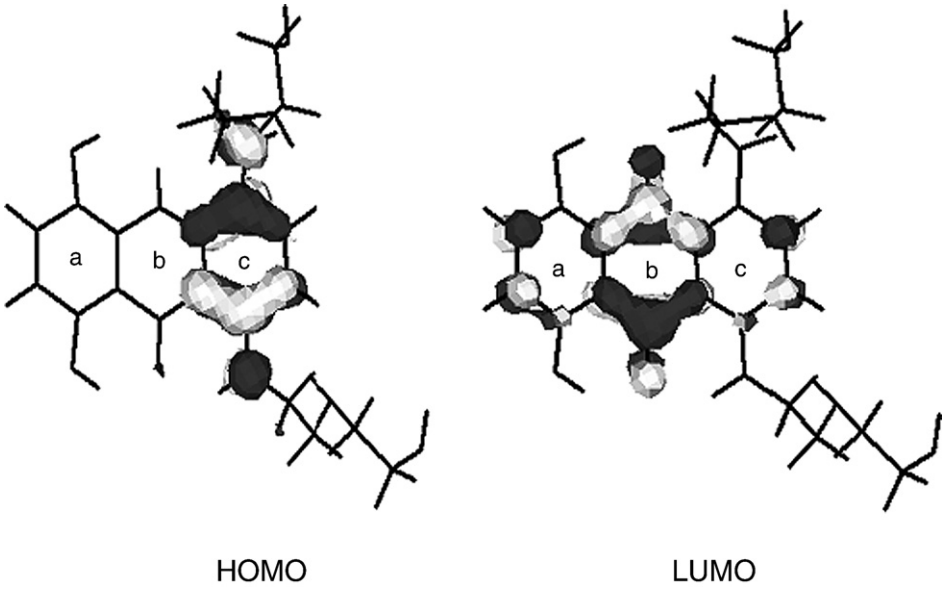

Fig. 7. The shape of the frontier molecular orbitals (HOMO and LUMO) of mitoxantrone.

Table 4
PM3 calculated reaction enthalpies, $\Delta^r H$, for the electron transfer reactions from the anion radical ($AH_2^{-\cdot}$) and dianion (AH_2^{2-}) of mitoxantrone to molecular oxygen, in gas phase and DMSO

Reaction	O_2 [a]	$\Delta^r H$ (kJ/mol) [b] (gas phase)	$\Delta^r H$ (kJ/mol) [b] (DMSO)
$AH_2^{-\cdot}+O_2 \rightarrow AH_2+O_2^{-\cdot}$	$^1\Delta_g$	95.74	−150.63
	$^3\Sigma_g$	190.26	−61.25
$AH_2^{2-}+O_2 \rightarrow AH_2^{-\cdot}+O_2^{-\cdot}$	$^1\Delta_g$	−225.25	−204.59
	$^3\Sigma_g$	−130.72	−115.22

[a] For molecular oxygen species the following ΔH^f values were used: −17.51 ($^3\Sigma_g$), 77.01 ($^1\Delta_g$) for gas phase, and −18.31 ($^3\Sigma_g$), 71.06 ($^1\Delta_g$) for DMSO; for $O_2^{-\cdot}$: −55.60 (gas phase) and −462.22 kJ/mol (DMSO).
[b] $\Delta^r H = \Sigma\ \Delta H^f_{Prod} - \Sigma\ \Delta H^f_{React}$.

quinone diimine, although the structure of the HOMO indicates as more probable the oxidation to the quinone-diimine structure. The differences in the reduction enthalpies of diquinone and quinone diimine to the corresponding anion radicals and dianions are greater, especially in DMSO, suggesting that these species may be involved in generation of free radicals.

4.1.3. Reactivity towards molecular oxygen

In regard with the possibility of the reductive activation of molecular oxygen, the energetics of the ET-reactions in Table 4 was examined for both ground ($^3\Sigma_g$) and singlet ($^1\Delta_g$) state of molecular oxygen, in gas phase and DMSO, using RHF heats of formation. The reductive activation of molecular oxygen to the superoxide anion is not energetically favourable from the anion radical of mitoxantrone in the gas phase but is exothermic in DMSO. Electron transfer from the dianion of mitoxantrone to both states of molecular oxygen is energetically favourable, suggesting that the dianion could play an important role in the redox cycling of this drug.

For diquinone and quinone diimine, the electron transfer from the anion radical and dianion to the ground state of molecular oxygen, in both gas phase and DMSO, is more favourable for quinone diimine (i.e. from the dianion in DMSO, the RHF calculated values are −74.07 kJ/mol for diquinone and −95.86 kJ/mol for quinone diimine).

The reduction potential of mitoxantrone is too negative to permit involvement of the drug in reductive activation by reductases, mitoxantrone being therefore less effective in the formation of free radicals and presenting a smaller cardiotoxicity. However, experimental and theoretical data indicate that the monoelectronic reduction of diquinone or quinone diimine (resulting compounds after bielectronic oxidation of mitoxantrone) is more favourable compared with mitoxantrone, and therefore these structures may be involved in other electron transfer processes and generation of toxic reactive oxygen species.

In conclusion, it may be stated that, although this attempt to rationalize the experimental results by means of semiempirical calculations is only a simplified thermodynamic approach, the use of electrochemical and spectral (EPR, absorption spectroscopy) methods in conjunction with theoretical MO calculations seems to be promising in the understanding of the reductive activation and cardiotoxicity of anti-cancer drugs.

References

[1] H. Lenk, U. Muller, S. Tanneberger, Mitoxantrone: mechanism of action, antitumor activity, pharmacokinetics, efficacy in the treatment of solid tumors and lymphomas, and toxicity, Anticancer Res. 7 (1987) 1257–1264.
[2] R.C. Stuart-Harris, I.E. Smith, Mitoxantrone: a phase II study in the treatment of patients with advanced breast carcinoma and other solid tumours, Cancer Chemother. Pharmacol. 8 (1982) 179–182.
[3] J. Kapuscinski, Z. Darzynkiewicz, Interactions of antitumor agents ametantrone and mitoxantrone (novantrone) with double-stranded DNA, Biochem. Pharmacol. 34 (1985) 4203–4213.
[4] G. Minotti, P. Menna, E. Salvatorelli, G. Cairo, L. Gianni, Anthracyclines: molecular advances and pharmacologic developments in antitumor activity and cardiotoxicity, Pharmacol. Rev. 56 (2004) 185–229.
[5] P.L. Gutierrez, The metabolism of quinone-containing alkylating agents: free radical production and measurement, Front. Biosci. 5 (2000) 629–638.
[6] J.H. Doroshow, K.J.A. Davies, Redox cycling of anthracyclines by cardiac mitochondria II. Formation of superoxide anion, hydrogen peroxide, and hydroxyl radical, J. Biol. Chem. 261 (1986) 3068–3074.
[7] B. Nguyen, P.L. Gutierrez, Mechanism(s) for the metabolism of mitoxantrone: electron spin resonance and electrochemical studies, Chem. Biol. Interact. 74 (1990) 139–162.
[8] X. Thomas, Q.H. Le, D. Fiere, Anthracycline-related toxicity requiring cardiac transplantation in long-term disease free survivors with acute promyelocytic leukemia, Ann. Hematol. 81 (2002) 504–507.
[9] R.E. Gonsette, Mitoxantrone in progressive multiple sclerosis: when and who to treat? J. Neurol. Sci. 206 (2003) 203–208.
[10] F.C. de Abreu, P.A. de L. Ferraz, M.O.F. Goulart, Some applications of electrochemistry in biomedical chemistry. Emphasis on the correlation of electrochemical and bioactive properties, J. Braz. Chem. Soc. 13 (2002) 19–35.
[11] N.C. Santos, J. Figueira-Coelho, J. Martins-Silva, C. Saldanha, Multidisciplinary utilization of dimethyl sulfoxide: pharmacological, cellular, and molecular aspects, Biochem. Pharmacol. 65 (2003) 1035–1041.
[12] I.B. Goldberg, A.J. Bard, Simultaneous electrochemical-electron spin resonance measurements I. Cell design and preliminary results, J. Phys. Chem. 75 (1971) 3281–3290.
[13] M. Ciureanu, M. Hillebrand, E. Volanschi, Cyclic voltammetry and spectral study of the electrochemical reduction of some dibenz-[b,e]-thiepinone derivatives, J. Electroanal. Chem. 291 (1990) 201–215.
[14] http://epr.niehs.nih.gov/pest.html.
[15] A. Klamt, G. Schuumann, COSMO: a new approach to dielectric screening in solvents with explicit expressions for the screening energy and its gradient, J. Chem. Soc. Perkin Trans. 2 (1993) 799–805.
[16] R.S. Nicholson, Theory and application of cyclic voltammetry for measurement of electrode reaction kinetics, Anal. Chem. 37 (1965) 1351–1355.
[17] A.J. Bard, L.R. Faulkner, Electrochemical methods. Fundamentals and Applications, J. Wiley & Sons. Inc., 2001, pp. 339–341.
[18] C. Frontana, I. Gonzales, The role of intramolecular hydrogen bonding in the electrochemical behavior of hydroxy-quinones and in semiquinone stability, J. Mex. Chem. Soc. 49 (2005) 61–69.
[19] J. William Lown, Hsiao-Hsiung Chen, Electron paramagnetic resonance characterization and conformation of daunorubicin semiquinone intermediate implicated in anthracycline metabolism, cardiotoxicity and anticancer action, Can. J. Chem. 59 (1981) 3212–3217.
[20] J.A. Weil, J.R. Bolton, J.E. Wertz, Electron paramagnetic resonance: elementary theory and practical applications, J. Wiley & Sons. Inc., 1994, pp. 239–259.
[21] E. Ionescu, M. Hillebrand, E. Volanschi, Experimental and theoretical study of the radicalic species obtained from alkylamino-2,4-dinitrobenzenes, Rev. Roum. Chim. 42 (1997) 897–905.
[22] M. Newcomb, M.T. Burchill, Origin of benzophenone ketyl in reactions of benzophenone with lithium dialkylamides. Implications for other possible electron transfer reactions, J. Am. Chem. Soc. 106 (1984) 8276–8282.
[23] E. Volanschi, M. Enache, E. Dinca, I. Serbanescu, Spectroelectrochemical study and MO-modeling of the reductive activation of antitumoral drug actinomycin D, Rev. Roum. Chim. 47 (2002) 741–750.
[24] I. Serbanescu, M. Enache, E. Volanschi, Electrochemical, spectral and MO investigation of the reductive activation of antitumoral drugs doxorubicin and epirubicin, Analele Universitatii Bucuresti I–II (2003) 267–278.

[25] A. Sawyer, E. Sullivan, Y.H. Mariam, A semiempirical computational study of electron transfer reactivity of one-vs. two-ring model systems for anthracycline pharmacopheres. I. A rationale for mode of action, J. Comput. Chem. 17 (1996) 204–225.
[26] Y.H. Mariam, A. Sawyer, A computational study on the relative reactivity of reductively activated 1,4-benzoquinone and its isolectronic analogs, J. Comput.-Aided Mol. Des. 10 (1996) 441–460.
[27] C. Bendic, M. Enache, E. Volanschi, Analysis of actinomycin D-DNA model complexes using a quantum-chemical criterion: Mulliken overlap populations, J. Mol. Graph. Mod. 24 (2005) 10–16.
[28] C. Bendic, E. Volanschi, Molecular modeling of the interaction of some phenoxazone-antitumoral drugs with DNA, Internet Electron. J. Mol. Des. 5 (2006) 320–330.
[29] S. Ozalp-Yaman, A.M. Onal, L. Turker, Electrochemical and quantum chemical studies on mitomycin and adriamycin, J. Mol. Struct. 654 (2003) 81–93.